JPET Fast Forward. Published on August 9, 2018 as DOI: 10.1124/jpet.118.250068
This article has not been copyedited and formatted. The final version may differ from this version.

PBI-4050 reduces stellate cell activation and liver fibrosis through modulation of intracellular ATP levels and LKB1-AMPK-mTOR pathway

Brigitte Grouix, Francois Sarra-Bournet, Martin Leduc, Jean-Christophe Simard, Kathy Hince, Lilianne Geerts, Alexandra Blais, Liette Gervais, Alexandre Laverdure, Alexandra Felton, Jonathan Richard, Jugurtha Ouboudinar, William Gagnon, François Leblond, Pierre Laurin and Lyne Gagnon

Prometic BioSciences Inc, Laval, Québec, Canada (BG, FSB, ML, JCS, KH, Lil.G, AB, Lie.G, AL, AF, JR, JO, WG, FL, PL, Ly.G)

JPET Fast Forward. Published on August 9, 2018 as DOI: 10.1124/jpet.118.250068
This article has not been copyedited and formatted. The final version may differ from this version.
JPET#250068

Running Title: PBI-4050 reduces liver fibrosis

Corresponding Author: Lyne Gagnon, PhD

Prometic BioSciences Inc.

500, boulevard Cartier Ouest (Suite 150), Laval, Québec, H7V 5B7, Canada

Telephone: +1-450-781-0115;

Fax: +1-450-781-1403

E-mail: l.gagnon@prometic.com

Number of text pages: 25

Number of figures: 8

Number of references: 47

Abstract word count: 253

Introduction word count: 501

Discussion word count: 922

List of abbreviations: Human hepatic stellate cells (HSCs), Serum aspartate aminotransferase (AST), Carbon tetrachloride (CCl_4), Bile duct ligation (BDL), Nitric oxide synthase (iNOS), Peroxisome proliferator-activated receptor γ (PPARγ), Liver kinase B1 (LKB1), AMP-activated protein kinase (AMPK), Alpha smooth muscle actin (α-SMA), connective tissue growth factor (CTGF), 5-aminoimidazole-4-carboxamide ribonucleotide (AICAR)

Recommended section: Gastrointestinal, Hepatic, Pulmonary and Renal

JPET Fast Forward. Published on August 9, 2018 as DOI: 10.1124/jpet.118.250068
This article has not been copyedited and formatted. The final version may differ from this version.
JPET#250068

ABSTRACT

Hepatic fibrosis is a major cause of morbidity and mortality for which there is currently no effective therapy. We have previously shown that PBI-4050 is a dual GPR40 agonist/GPR84 antagonist exerting anti-fibrotic, anti-inflammatory and anti-proliferative actions. We evaluated PBI-4050 for the treatment of liver fibrosis in vivo and elucidated its mechanism of action on human hepatic stellate cells (HSCs). The anti-fibrotic effect of PBI-4050 was evaluated in carbon tetrachloride and in bile duct ligation-induced liver fibrosis rodent models. Treatment with PBI-4050 suppressed CCl_4-induced serum aspartate aminotransferase level, inflammatory marker nitric oxide synthase, epithelial to mesenchymal transition transcription factor Snail and multiple pro-fibrotic factors. PBI-4050 also decreased GPR84 mRNA expression in CCl_4-induced injury, while restoring PPARγ to the control level. In a bile duct ligation rat model, collagen deposition and α-SMA protein level were also attenuated by PBI-4050 treatment. TGF-β-activated primary HSCs were used to examine the effect of PBI-4050 and its mechanism of action in vitro. PBI-4050 inhibited the proliferation of HSCs by arresting the cells in a G0/G1 cycle phase. Subsequent analysis demonstrated that PBI-4050 signals through reduction of intracellular ATP levels, activation of LKB1 and AMPK, and blocking of mTOR, resulting in reduced protein and mRNA levels of α-SMA and CTGF, and restoration of PPARγ mRNA expression. Our findings suggest that PBI-4050 may exert its anti-fibrotic activity in the liver through a novel mechanism of action involving modulation of intracellular ATP levels and LKB1-AMPK-mTOR pathway in stellate cells and suggests that PBI-4050 may be a promising agent for treating liver fibrosis.

JPET Fast Forward. Published on August 9, 2018 as DOI: 10.1124/jpet.118.250068
This article has not been copyedited and formatted. The final version may differ from this version.
JPET#250068

INTRODUCTION

Hepatic fibrosis is a major cause of morbidity and mortality worldwide. Fibrosis, a wound-healing response to chronic liver injury, is characterized by excessive overproduction and deposition of extracellular matrix (ECM) (Friedman, 2008; Schuppan and Kim, 2013). During fibrogenesis, HSCs are activated and transdifferentiate into proliferative, myofibroblast-like cells which are the major cell type responsible for ECM synthesis and accumulation (Bataller and Brenner, 2005). Transformation of HSCs to myofibroblasts is characterized by several phenotypic changes such as overexpression of α-SMA, secretion of pro-fibrotic mediators including connective tissue growth factor (CTGF) (Friedman, 2000), loss of expression of peroxisome proliferator-activated receptor γ (PPARγ), a transcription factor essential for HSCs differentiation (Kweon et al., 2016), and secretion of type I collagen (Henderson and Iredale, 2007). Therefore, modulating HSCs activation may be a potential anti-fibrosis therapy.

Recent studies have reported a close relationship between AMP-activated protein kinase (AMPK), a cellular energy sensor, and hepatic fibrosis (Liang et al., 2017). It was found that activation of AMPK inhibits TGF-β-mediated activation of cultured HSCs (Lim et al., 2012), and activation of AMPK has been a target of various anti-fibrosis therapies. Direct AMPK activator 5-aminoimidazole-4-carboxamide ribonucleotide (AICAR) and indirect AMPK activators such as metformin, berberine, or cucurbitacin E have been reported to have anti-fibrotic activity in both activated HSCs and animal models of hepatic fibrosis such as the CCl_4-induced liver injury or the BDL rodent models (Leclerc et al., 2010; Kumar et al., 2014; Li et al., 2014; Tripathi et al., 2015; Wang et al., 2016; Wu et al., 2016).

We have previously shown that PBI-4050 is a synthetic agonist of GPR40 (EC_{50} of 288 and 30 μM for activation of GPR40/$G\alpha_q$ and $G\alpha_{i2}$, respectively) and antagonist of GPR84 (IC_{50} of 398 and 209 μM for inhibition of sodium decanoate- and embelin-induced activation of GPR84/$G\alpha_{i2}$, respectively) (Gagnon et al., 2018). GPR40 and GPR84 are both fatty acid binding receptors; GPR40 is activated by both medium-chain and long-chain fatty acids (Briscoe et al., 2003) while GPR84 binds only to medium-chain fatty acids (Wang et al., 2006). We have recently reported that GPR40 KO mice are more prone to renal injury-induced fibrosis while GPR84 KO mice are protected, and that PBI-4050 has anti-fibrotic activity in various animal

JPET Fast Forward. Published on August 9, 2018 as DOI: 10.1124/jpet.118.250068
This article has not been copyedited and formatted. The final version may differ from this version.
JPET#250068

models of tissue fibrosis as well as in fibroblast and epithelial cells (Gagnon et al., 2018). Moreover, PBI-4050 inhibits TGF-β-induced activation of normal human dermal fibroblasts to pro-fibrotic myofibroblasts, as demonstrated by abrogation of α-SMA, CTGF and collagen I expression.

Based on PBI-4050 anti-fibrotic activity previously reported, we hypothesized that PBI-4050 may have a protective effect on hepatic fibrosis. In the present study, the anti-fibrotic activity of PBI-4050 was evaluated in a CCl_4-induced liver injury animal model, an extensively used model in experimental studies showing many shared characteristics with human fibrosis (Weiler-Normann et al., 2007). We also confirmed PBI-4050 anti-fibrotic activity in a BDL rat model of hepatic fibrosis (Biecker et al., 2005). Furthermore, we uncovered a novel mechanism of action of PBI-4050 in activated human HSCs involving modulation of intracellular ATP levels and LKB1-AMPK-mTOR pathway.

JPET Fast Forward. Published on August 9, 2018 as DOI: 10.1124/jpet.118.250068
This article has not been copyedited and formatted. The final version may differ from this version.

MATERIAL AND METHODS

Reagents – Carbon tetrachloride (CCl_4) was obtained from Sigma. HSCs and medium (SteCM) were obtained from ScienCell. Pierce Coomassie protein assay kit was purchased from Bio-Rad. Human CTGF ELISA kit was from Origene. PBI-4050 was synthesized as previously described (Gagnon et al., 2018).

Cell culture – HSCs were cultured in SteCM with 2% FBS plus stellate cell growth supplement and penicillin/streptomycin solution. Cells were starved 4 h in medium with 0.4% FBS and treated with or without recombinant human TGF-β1 (Biolegend) at 10 ng/ml, PDGF-BB at 10 ng/mL (R&D systems) and PBI-4050 for 24 h. Cells were then processed for qPCR, Western blot, and supernatants collected for CTGF ELISA.

Animal studies – All animal studies were reviewed and approved by the animal care and ethic committee of INRS-Institut-Armand-Frappier.

CCl_4-induced liver fibrosis – Liver fibrosis was induced in 6-weeks old male C57BL/6 mice (Charles River) by intraperitoneal (i.p.) administration of 2 ml/kg of CCl_4 diluted at 10% in olive oil, twice a week for 58 days. Mice were randomly divided into 4 groups. Sham group was injected with an equal volume of olive oil i.p. and orally administered an equal volume of distilled water. CCl_4 group was injected i.p. with CCl_4 and administered an equal volume of vehicle (distilled water) instead of PBI-4050. PBI-4050 at either 100 mg/kg or 200 mg/kg was orally administered from day 1 to day 58 to CCl_4-treated mice. Mice were sacrificed at day 59. Livers were collected to evaluate fibrosis, and blood samples for liver enzyme assay.

Bile duct ligation-induced fibrosis – Cholestasis and resulting inflammatory liver disease were induced by a double ligation of the common bile duct (BDL) of male Wistar rats by abdominal laparotomy under isoflurane anesthesia. Silk sutures were tied around the isolated BDL at cranial and caudal ends and the BDL was transected between the ligatures. Animals were kept under normal housing condition for up to 8 weeks.

JPET Fast Forward. Published on August 9, 2018 as DOI: 10.1124/jpet.118.250068
This article has not been copyedited and formatted. The final version may differ from this version.

Liver enzyme assay – Serum aspartate transaminase (AST) activity was determined at time of sacrifice using the EnzyChrome Aspartate Transaminase Assay kit (Bioassay Systems).

Western Blotting – Total proteins were extracted from liver tissue and HSCs with lysis buffer. 20µg of protein were separated by standard SDS-PAGE techniques and immunoblotted with the following antibodies: rabbit anti-AMPKα (1:1000), rabbit anti-phospho-AMPK Thr172 (1:1000), rabbit anti-LKB1 (1:1000), rabbit anti-phospho-LKB1 Ser428 (1:1000), rabbit anti-mTOR (1:1000), rabbit anti-phospho-mTOR Ser2448 (1:1000), goat anti-rabbit secondary antibody (1:1000) were from Cell Signaling Technology. Rabbit anti-α-SMA antibody (1:200) was from Abcam and anti-GAPDH (1:1000) from Santa Cruz. Chemiluminescence was revealed with a ChemiDoc MP imaging system (Bio-Rad) and densitometric analyses of Western blot were performed using ImageLab version 5.2.1 (Bio-Rad). Phospho-AMPK, phospho-LKB1, and phospho-mTOR signal was normalized to their respective total proteins and α-SMA was normalized to GAPDH or on total protein lane (MemCode protein stain kit, Fisher Scientific).

Cell Cycle – HSCs were treated 24h in complete medium, harvested and fixed in ice-cold 70% ethanol for 30 min at 4°C. HSCs were washed twice in PBS, centrifuged, and resuspended in Krishan buffer containing 0.1% sodium citrate, 50 µg/mL RNase A, 50 µg/mL propidium iodide (PI) and 0.2% NP-40. HSCs were incubated 60 minutes and cell cycle was analyzed on a FACS Calibur flow cytometer (BD Biosciences). Results were analyzed using Flowing Software (version 2.5.1).

Cell proliferation – HSCs were seeded in complete medium in two separate 96-well plates at a density of 4 x 10^3 cells/well for attachment overnight. Resazurin (Sigma) was added to control plate (time 0) and fluorescence was read 4 hours later at 535(ex)/595(em) nm with a gain of 80. HSCs in the other plate were treated with or without TGF-β1 or PDGF-BB and PBI-4050 for 20 hours before addition of resazurin. Four hours later fluorescence was read at 535(ex) /595(em) nm with a gain of 80. Results were analyzed and expressed as percentage of time 0.

JPET Fast Forward. Published on August 9, 2018 as DOI: 10.1124/jpet.118.250068
This article has not been copyedited and formatted. The final version may differ from this version.

Intracellular ATP measurement – $1x10^6$ HSCs were plated in a 100 mm culture dish for attachment overnight. Cells were starved 4 h in medium with 0.4% FBS and treated with or without recombinant human TGF-β1 and PBI-4050 for 24 h. The ATP colorimetric/fluorometric assay kit (BioVision) was performed as per manufacturer recommendations, using $5x10^5$ cells.

Quantitative real-time PCR – RNA was extracted from cultured HSCs and homogenized liver tissue using the TRIzol reagent (Fisher Scientific) and treated with TURBO DNA-free DNase (Fisher Scientific) as per manufacturer's instructions. Extracted RNA was converted to cDNA using GoScript Reverse Transcriptase with 500-1000 ng starting material per reaction. Quantitative PCR (qPCR) was performed on an AB-7900HT real-time cycler using TaqMan gene expression assays (Life Technologies). qPCR data was analyzed using the ΔΔCt method, using GAPDH or HPRT1 as normalization controls for CCl_4 and HSCs respectively.

Hydroxyproline determination – 100 mg of tissue were homogenized in 1 mL of distilled water. 500 µl (50 mg of tissue) was transferred to a pressure-tight vial with PTFE-lined cap. 500 µl of concentrated hydrochloric acid (12 M) was added and tissues were hydrolyzed at 120°C overnight. 50 µl of supernatant of each sample was transferred to a 96 well plate and evaporated to dryness in a 60°C oven. Samples were oxidized in 1.4% chloramine T solution for 15 min at room temperature, after which 100 µl of Ehrlitch's solution was added. After 60 min incubation at 60°C, OD was read at 560 nm.

Histological image analysis – Liver injury was assessed in a blinded-manner. Paraffin slides were de-paraffinized, rehydrated and stained with Masson's trichrome or Picro-Sirius Red. Based on the distinctive density and color of staining in digital images, the area of collagen in the tissue was quantified using Image-Pro Premier 9.1. Sections from at least four regions of each organ were analyzed, and the average was used as data from one animal sample.

JPET Fast Forward. Published on August 9, 2018 as DOI: 10.1124/jpet.118.250068
This article has not been copyedited and formatted. The final version may differ from this version.

Statistics – Data are expressed as mean ± SEM for each treatment compared to control. Statistical analysis was performed using one-way ANOVA with Dunnett's post-test for multiple comparisons. All data were analyzed using GraphPad Prism version 7 for Windows (GraphPad, San Diego, CA, USA).

JPET Fast Forward. Published on August 9, 2018 as DOI: 10.1124/jpet.118.250068
This article has not been copyedited and formatted. The final version may differ from this version.
JPET#250068

RESULTS

PBI-4050 decreases collagen deposition in liver and AST serum levels in CCl_4-induced mice – To evaluate the degree of liver fibrosis in CCl_4-induced mice, collagen in liver tissue was determined by Masson's trichrome staining (Figure 1a and 1b). While CCl_4 induced collagen accumulation (blue staining) compared to Sham group, PBI-4050 significantly decreased the area of collagen in the liver. These results were confirmed by quantification of hydroxyproline level (Figure 1c) and collagen I gene expression (Figure 1d) in liver tissues, in which PBI-4050 remarkably protected against CCl_4-induced collagen accumulation. Moreover, CCl_4 administration resulted in an increased level of AST (Figure 1e), indicative of liver damage. Mice treated with PBI-4050 at 200 mg/kg completely prevented the increase of this enzyme when compared to the CCl_4 group.

PBI-4050 attenuates CCl_4-induced α-SMA activation in mice – Previous studies have shown that elevated expression of α-SMA is a marker of activated HSCs (Weiler-Normann et al., 2007) and is upregulated by CCl_4-treatment (Fan et al., 2017). Indeed, α-SMA staining was strongly increased in CCl_4-treated mice compared to Sham group, whereas it was markedly reduced in liver of PBI-4050-treated mice (Figure 2a). Protein levels of α-SMA in liver tissues were also analyzed by Western blot and corroborated that PBI-4050 treatment significantly decreased α-SMA compared to CCl_4 control mice (Figure 2b). Moreover, as shown in Figure 2c, PBI-4050 treatment also decreased the expression of α-SMA gene compared to CCl_4 mice.

PBI-4050 regulates gene expression of fibrosis/inflammation markers in liver of CCl_4 mice – We next investigated the changes in mRNA levels of fibrotic/matrix remodeling (MMP-2, TIMP-1, and Snail1) markers. A marked elevation of MMP-2, TIMP-1, and Snail1 mRNA levels was observed in CCl_4-treated mice and PBI-4050 suppressed the expression of these genes to the level of sham animals (Figure 3a-c). Large amounts of nitric oxide are generated by the proinflammatory marker iNOS in many liver diseases,

JPET Fast Forward. Published on August 9, 2018 as DOI: 10.1124/jpet.118.250068
This article has not been copyedited and formatted. The final version may differ from this version.
JPET#250068

including liver fibrosis, and iNOS inhibition has been considered as a therapeutic strategy in several diseases (Iwakiri, 2015). Indeed, CCl_4 mice showed higher iNOS expression which was reduced by PBI-4050 treatment (Figure 3d). PPARγ downregulation is a well-known marker of stellate cell activation (Hazra et al., 2004). Interestingly, PPARγ gene expression which was decreased by CCl_4 treatment was restored to the level of the sham group by PBI-4050 (Figure 3e). It has previously been shown that PBI-4050, through binding to GPR40 and GPR84, significantly attenuated fibrosis in various renal fibrosis models (Gagnon et al., 2018). The mRNA expression levels of GPR40 and GPR84 in liver were thus examined. GPR84 gene expression, which was upregulated in CCl_4 mice, was returned to normal levels by treatment with PBI-4050 (Figure 3f). No significant level of GPR40 mRNA was detected in the liver samples.

PBI-4050 attenuates hepatic fibrosis induced by BDL in rats

To confirm results observed in the CCl_4 fibrosis mouse model, we investigated the effect of PBI-4050 in BDL-induced hepatic fibrosis in rats. Histological analysis revealed that administration of PBI-4050 significantly decreased collagen deposition induced by BDL in rat livers (Figure 4 a,b), as seen in the CCl_4 mouse model (Figure 1). Protein levels of α-SMA in liver tissues were also analyzed by Western blot and PBI-4050 treatment considerably decreased α-SMA compared to BDL rats (Figure 3 c,d). Moreover, we also observed a strong upregulation of GPR84 gene expression following BDL (Supplemental Figure 1).

PBI-4050 inhibits cell proliferation and cell cycle progression in activated HSCs – HSCs are considered the most prominent cell type involved in liver fibrogenesis (Bataller and Brenner, 2005; Iredale, 2007; Wynn, 2007). Activated HSCs exhibit a strong proliferative activity (Puche et al., 2013). In our hands, TGF-β increased HSCs proliferation by 10 percent only as shown in Figure 5a, this might be due to partial activation of HSCs when they are grown on plastic substrate in tissue culture plates (Gutierrez-Ruiz and Gomez-Quiroz, 2007). Nevertheless, a 24 h treatment with PBI-4050 at 500 µM inhibited TGF-β-activated

JPET Fast Forward. Published on August 9, 2018 as DOI: 10.1124/jpet.118.250068
This article has not been copyedited and formatted. The final version may differ from this version.
JPET#250068

HSCs proliferation. This decreased cell proliferation was not associated to PBI-4050 cytotoxicity as proliferation of PBI-4050 treated HSCs was above the Time 0 baseline of untreated cells. To confirm these results, cell cycle analysis was performed on HSCs cultured for 24 hours in the presence or absence of TGF-β1 and PBI-4050. Figure 5b shows that PBI-4050 dose-dependently arrested HSCs at the G0/G1 phase without inducing apoptosis. Similarly, PBI-4050 also blocked HSCs stimulated with the potent proliferative agent PDGF-BB at the G0/G1 phase (Supplemental Figure 2).

PBI-4050 regulates the expression of fibrosis markers in activated HSCs – Stimulation of HSCs with TGF-β has been shown to induce a strong increase in the expression of the pro-fibrotic marker CTGF, leading to an increase in α-SMA (a myofibroblast marker) (Huang and Brigstock, 2012; Li et al., 2015). Therefore, CTGF and α-SMA expression was examined in PBI-4050-treated HSCs. TGF-β activation led to a robust increase of α-SMA and CTGF, both at the mRNA and protein levels. PBI-4050 treatment significantly and dose-dependently reduced the mRNA expression of theses markers (Figures 6a). In addition, protein levels of α-SMA (Figure 6b) and CTGF (Figure 6c) were drastically reduced by PBI-4050 treatment, returning to the level detected in untreated cells. Moreover, HSCs activation and differentiation have been associated with the transcription factor PPARγ. Expression of PPARγ, detectable in quiescent HSCs, is lacking in activated HSCs and myofibroblasts (Friedman, 2008; Bennett et al., 2017). As shown in Figure 6a, TGF-β1 reduced PPARγ expression in HSCs and PBI-4050 restored its expression in a dose-dependent manner.

PBI-4050 modulates the LKB1-AMPK-mTOR signaling pathway in activated HSCs – To further elucidate PBI-4050 mechanism of action in vitro, we studied its signaling pathway. GPR40 and GPR84 mRNA were below detection level in cultured quiescent or TGF-β-stimulated HSC, and we thus investigated alternative mechanisms of action in these cells. PBI-4050 did not modulate the TGF-β-induced canonical Smad2/3 signaling pathway in HSCs (Supplemental Figure 3). It was recently shown that AMPK modulates proliferation and inhibits TGF-β-induced fibrogenic properties of HSCs (da Silva Morais et al.,

JPET Fast Forward. Published on August 9, 2018 as DOI: 10.1124/jpet.118.250068
This article has not been copyedited and formatted. The final version may differ from this version.

2009). Based on our results we investigated whether the inhibitory effect of PBI-4050 on HSC activation and proliferation could involve phosphorylation of AMPK. As shown in Figure 7a, treatment with PBI-4050 at 500 μM significantly promoted phosphorylation of AMPK in TGF-β-activated HSC. To further elucidate the upstream signaling mechanism of AMPK activation by PBI-4050, phosphorylation of LKB1, a major upstream kinase in the AMPK cascade was examined (Fu et al., 2008). Our results show that PBI-4050 treatment increased LKB1 phosphorylation level (Figure 7b). It has been shown that AMPK activation leads to the modulation of the master regulator of growth mTOR (Herzig and Shaw, 2018). Consistent with the literature and AMPK activation by PBI-4050 treatment, we also demonstrated an inhibition of mTOR phosphorylation (Figure 7c). Activation of AMPK by LKB1 depends on the intracellular AMP/ATP ratio (Hardie, 2003; Hardie, 2004) Thus, we next measured the ATP concentration in TGF-β-activated HSC treated with PBI-4050. PBI-4050 significantly decreased intracellular ATP at doses of 250 and 500 μM (Figure 7d). Taken together, these results suggest that the inhibitory effect of PBI-4050 on HSC activation and proliferation is mediated by reduced intracellular ATP concentrations, activation of LKB1/AMPK, and inhibition of mTOR.

JPET Fast Forward. Published on August 9, 2018 as DOI: 10.1124/jpet.118.250068
This article has not been copyedited and formatted. The final version may differ from this version.
JPET#250068

DISCUSSION

In the present study, we clearly demonstrate the potential therapeutic effect of PBI-4050 in liver fibrosis. It is well known that liver fibrogenesis is accompanied by increased collagen deposition in the perisinusoidal and periportal spaces (Chu et al., 2016). During hepatic fibrogenesis, the TIMP-MMP balance is disturbed, and TIMPs are over-expressed contributing to ECM deposition and development of fibrosis (Iredale et al., 2013). Increased expression of TIMP-1 has been observed in both liver tissue and serum of patients with liver disease and in animal models of liver fibrosis (Thiele et al., 2017). PBI-4050 was efficacious in reducing collagen and other fibrotic markers (α-SMA and CTGF) at the mRNA expression and protein levels in the CCl_4-induced hepatotoxicity murine model and reduced collagen deposition and α-SMA in the bile duct ligation rat model. In addition, PBI-4050 induced a marked inhibition of ECM remodeling markers MMP2 and TIMP-1 in CCl_4-treated animals as well as negative modulation of the EMT-related transcription factor Snail1. Expression of the proinflammatory mRNA marker iNOS was also returned to normal in PBI-4050-treated livers. Several natural compounds such as Morin, a plant-derived flavonoid, have been shown to ameliorate liver fibrosis by suppressing iNOS (Dhanasekar and Rasool, 2016). Finally, treatment with PBI-4050 improved liver function as observed with the reduction of AST activity in CCl_4-induced mice.

In the liver, HSC are the major cellular source of ECM. In response to liver injury, hepatocytes, Kupffer cells, and platelets secrete TGF-β which activates HSCs in a paracrine fashion (Gressner and Weiskirchen, 2006). Quiescent HSCs undergo a process of trans-differentiation into activated HSC/myofibroblasts expressing α-SMA (Weiler-Normann et al., 2007). In our study, PBI-4050 was shown to induce a strong reduction of α-SMA expression at both protein and mRNA levels in activated HSCs. These results further strengthen the observed antifibrotic activity of PBI-4050 in preclinical models.

Subsequent signaling analysis in activated HSCs demonstrated that PBI-4050 modulated intracellular ATP and the LKB1/AMPK/mTOR pathway. PBI-4050 displayed more potent effects on lowering intracellular ATP and mTOR phosphorylation than it did on increasing LKB1 and AMPK phosphorylation (only the

JPET Fast Forward. Published on August 9, 2018 as DOI: 10.1124/jpet.118.250068
This article has not been copyedited and formatted. The final version may differ from this version.

500 μM dose of PBI-4050 significantly modulated the latter). These results suggest that inhibition of mTOR activation could be a consequence of several pathways depending of PBI-4050 concentration, including activation of the LKB1/AMPK pathway, and decreased direct binding of ATP to mTOR. Indeed, mTOR has an ATP-binding pocket and is an ATP sensor (Dennis et al., 2001; Yang et al., 2013) . It has also been shown that phosphorylation of mTOR at serine-2448, measured in the present study, can be regulated as a feedback signal to mTOR from its major downstream target, p70S6 kinase (Chiang and Abraham, 2005).

Interestingly, the inhibition of HSCs proliferation through a G0/G1 cell cycle arrest induced by PBI-4050 corroborates with previous work showing that activation of AMPK could suppress HSCs proliferation (Gressner and Weiskirchen, 2006). It has also been reported that AMPK stimulation negatively controls the expression of α-SMA and other markers of fibrosis in HSCs (da Silva Morais et al., 2009; Lee et al., 2016), in agreement with our results in PBI-4050-treated HSCs. There is increasing evidence showing a beneficial role of AMPK activation in reducing hepatic fibrosis, improving liver function, and lowering hepatocytotoxicity (Liang et al., 2017), and several novel drug candidates for the treatment of hepatic fibrosis, including metformin, betulin, berberine, cucurbitacin E, and curcumin, have been shown to act via increased AMPK signaling (Xu et al., 2003; Fu et al., 2008; Yang et al., 2015; Wu et al., 2016; Liang et al., 2017). Moreover, AMPK-signaling is known to negatively regulate mTOR, an atypical serine/threonine kinase that has been shown to play an important role in the regulation of cell growth, differentiation, migration, and survival through S6K1, 4EBP1 and PPARγ transcription factors. mTOR inhibitors have become a target to suppress the activation of HSC and liver fibrosis (Zhai et al., 2015).

It has been shown that PPARγ is a critical transcription factor involved in the inhibition of HSCs activation (Hazra et al., 2004; Zhai et al., 2015). Interestingly, PBI-4050 restored PPARγ expression which was downregulated in TGF-β-activated HSCs and in CCl_4 liver extracts. Upregulation of PPARγ has also been shown to be associated with increased phospho-AMPK and decreased phospho-mTOR (Zhong et al., 2018). Additional studies are required to further elucidate the mechanism of action of PBI-4050 in TGF-β-activated HSCs, especially by investigating downstream effectors of mTOR that control cell growth and

JPET Fast Forward. Published on August 9, 2018 as DOI: 10.1124/jpet.118.250068
This article has not been copyedited and formatted. The final version may differ from this version.

protein synthesis as well as autophagy; however, PBI-4050 did not have any effect on canonical TGF-β signaling through Smad2/3 phosphorylation in HSCs (Supplemental Figure 3).

Furthermore, although GPR40 and GPR84 were not expressed in cultured quiescent or TGF-β-stimulated HSCs, other stimuli like TNF-α and LPS (that could be found in an in vivo pathological context) induced mRNA expression of GPR84 in HSCs (Supplemental Figure 4). Our previous work has shown an upregulation of renal GPR84 expression and a profibrotic role of GPR84 in kidney fibrosis models (Gagnon et al., 2018). Increased GPR84 expression was also observed in the CCl_4 model and may be linked to the increase in fibrosis, as PBI-4050 treatment decreased both GPR84 expression and fibrosis in this model. Further work is required to determine the precise role of GPR84 in liver fibrogenesis.

Figure 8 summarizes the preliminary novel signalling pathway of PBI-4050 extracted from the data obtained in HSCs and the CCl_4-induced liver fibrosis model. The antifibrotic and antiproliferative activity of PBI-4050 on activated HSCs seemed to be mediated through the modulation of intracellular ATP and the LKB1-AMPK-mTOR-PPARγ signaling axis, resulting in regulation of hepatic ECM deposition and remodeling, and in decreased liver fibrosis.

JPET Fast Forward. Published on August 9, 2018 as DOI: 10.1124/jpet.118.250068
This article has not been copyedited and formatted. The final version may differ from this version.
JPET#250068

AUTHOR CONTRIBUTIONS

Participated in research design: Grouix, Sarra-Bournet, Laurin, L. Gagnon

Conducted experiments: Sarra-Bournet, Hince, Geerts, Blais, Simard, Gervais, Laverdure, Felton, Richard, Ouboudinar, W. Gagnon

Performed data analysis: Sarra-Bournet, Hince, Geerts, Blais, Simard, Gervais, Laverdure, Leblond, Grouix

Wrote or contributed to the writing of the manuscript: Grouix, Sarra-Bournet, Leduc, Simard, L. Gagnon

JPET Fast Forward. Published on August 9, 2018 as DOI: 10.1124/jpet.118.250068
This article has not been copyedited and formatted. The final version may differ from this version.
JPET#250068

References

Bataller R and Brenner DA (2005) Liver fibrosis. *J Clin Invest* **115**:209-218.

Bennett RG, Simpson RL and Hamel FG (2017) Serelaxin increases the antifibrotic action of rosiglitazone in a model of hepatic fibrosis. *World J Gastroenterol* **23**:3999-4006.

Biecker E, De Gottardi A, Neef M, Unternahrer M, Schneider V, Ledermann M, Sagesser H, Shaw S and Reichen J (2005) Long-term treatment of bile duct-ligated rats with rapamycin (sirolimus) significantly attenuates liver fibrosis: analysis of the underlying mechanisms. *J Pharmacol Exp Ther* **313**:952-961.

Briscoe CP, Tadayyon M, Andrews JL, Benson WG, Chambers JK, Eilert MM, Ellis C, Elshourbagy NA, Goetz AS, Minnick DT, Murdock PR, Sauls HR, Jr., Shabon U, Spinage LD, Strum JC, Szekeres PG, Tan KB, Way JM, Ignar DM, Wilson S and Muir AI (2003) The orphan G protein-coupled receptor GPR40 is activated by medium and long chain fatty acids. *J Biol Chem* **278**:11303-11311.

Chiang GG and Abraham RT (2005) Phosphorylation of mammalian target of rapamycin (mTOR) at Ser-2448 is mediated by p70S6 kinase. *J Biol Chem* **280**:25485-25490.

Chu X, Wang H, Jiang YM, Zhang YY, Bao YF, Zhang X, Zhang JP, Guo H, Yang F, Luan YC and Dong YS (2016) Ameliorative effects of tannic acid on carbon tetrachloride-induced liver fibrosis in vivo and in vitro. *J Pharmacol Sci* **130**:15-23.

da Silva Morais A, Abarca-Quinones J, Guigas B, Viollet B, Starkel P, Horsmans Y and Leclercq IA (2009) Development of hepatic fibrosis occurs normally in AMPK-deficient mice. *Clin Sci (Lond)* **118**:411-420.

Dennis PB, Jaeschke A, Saitoh M, Fowler B, Kozma SC and Thomas G (2001) Mammalian TOR: a homeostatic ATP sensor. *Science* **294**:1102-1105.

Dhanasekar C and Rasool M (2016) Morin, a dietary bioflavonol suppresses monosodium urate crystal-induced inflammation in an animal model of acute gouty arthritis with reference to NLRP3

inflammasome, hypo-xanthine phospho-ribosyl transferase, and inflammatory mediators. *Eur J Pharmacol* **786**:116-127.

Fan K, Wu K, Lin L, Ge P, Dai J, He X, Hu K and Zhang L (2017) Metformin mitigates carbon tetrachloride-induced TGF-beta1/Smad3 signaling and liver fibrosis in mice. *Biomed Pharmacother* **90**:421-426.

Friedman SL (2000) Molecular regulation of hepatic fibrosis, an integrated cellular response to tissue injury. *J Biol Chem* **275**:2247-2250.

Friedman SL (2008) Hepatic stellate cells: protean, multifunctional, and enigmatic cells of the liver. *Physiol Rev* **88**:125-172.

Fu Y, Zheng S, Lin J, Ryerse J and Chen A (2008) Curcumin protects the rat liver from CCl4-caused injury and fibrogenesis by attenuating oxidative stress and suppressing inflammation. *Mol Pharmacol* **73**:399-409.

Gagnon L, Leduc M, Thibodeau JF, Zhang MZ, Grouix B, Sarra-Bournet F, Gagnon W, Hince K, Tremblay M, Geerts L, Kennedy CRJ, Hebert RL, Gutsol A, Holterman CE, Kamto E, Gervais L, Ouboudinar J, Richard J, Felton A, Laverdure A, Simard JC, Letourneau S, Cloutier MP, Leblond FA, Abbott SD, Penney C, Duceppe JS, Zacharie B, Dupuis J, Calderone A, Nguyen QT, Harris RC and Laurin P (2018) A Newly Discovered Antifibrotic Pathway Regulated by Two Fatty Acid Receptors: GPR40 and GPR84. *Am J Pathol* **188**:1132-1148.

Gressner AM and Weiskirchen R (2006) Modern pathogenetic concepts of liver fibrosis suggest stellate cells and TGF-beta as major players and therapeutic targets. *J Cell Mol Med* **10**:76-99.

Gutierrez-Ruiz MC and Gomez-Quiroz LE (2007) Liver fibrosis: searching for cell model answers. *Liver Int* **27**:434-439.

Hardie DG (2003) Minireview: the AMP-activated protein kinase cascade: the key sensor of cellular energy status. *Endocrinology* **144**:5179-5183.

Hardie DG (2004) The AMP-activated protein kinase pathway--new players upstream and downstream. *J Cell Sci* **117**:5479-5487.

Hazra S, Xiong S, Wang J, Rippe RA, Krishna V, Chatterjee K and Tsukamoto H (2004) Peroxisome proliferator-activated receptor gamma induces a phenotypic switch from activated to quiescent hepatic stellate cells. *J Biol Chem* **279**:11392-11401.

Henderson NC and Iredale JP (2007) Liver fibrosis: cellular mechanisms of progression and resolution. *Clin Sci (Lond)* **112**:265-280.

Herzig S and Shaw RJ (2018) AMPK: guardian of metabolism and mitochondrial homeostasis. *Nat Rev Mol Cell Biol* **19**:121-135.

Huang G and Brigstock DR (2012) Regulation of hepatic stellate cells by connective tissue growth factor. *Front Biosci (Landmark Ed)* **17**:2495-2507.

Iredale JP (2007) Models of liver fibrosis: exploring the dynamic nature of inflammation and repair in a solid organ. *J Clin Invest* **117**:539-548.

Iredale JP, Thompson A and Henderson NC (2013) Extracellular matrix degradation in liver fibrosis: Biochemistry and regulation. *Biochim Biophys Acta* **1832**:876-883.

Iwakiri Y (2015) Nitric oxide in liver fibrosis: The role of inducible nitric oxide synthase. *Clin Mol Hepatol* **21**:319-325.

Kumar P, Smith T, Rahman K, Thorn NE and Anania FA (2014) Adiponectin agonist ADP355 attenuates CCl4-induced liver fibrosis in mice. *PLoS One* **9**:e110405.

Kweon SM, Chi F, Higashiyama R, Lai K and Tsukamoto H (2016) Wnt Pathway Stabilizes MeCP2 Protein to Repress PPAR-gamma in Activation of Hepatic Stellate Cells. *PLoS One* **11**:e0156111.

Leclerc GM, Leclerc GJ, Fu G and Barredo JC (2010) AMPK-induced activation of Akt by AICAR is mediated by IGF-1R dependent and independent mechanisms in acute lymphoblastic leukemia. *J Mol Signal* **5**:15.

Lee HS, Shin HS, Choi J, Bae SJ, Wee HJ, Son T, Seo JH, Park JH, Kim SW and Kim KW (2016) AMP-activated protein kinase activator, HL156A reduces thioacetamide-induced liver fibrosis in mice and inhibits the activation of cultured hepatic stellate cells and macrophages. *Int J Oncol* **49**:1407-1414.

Li J, Dong N, Cheng S, Li X, Wang W and Xiang Y (2015) Tetramethylpyrazine inhibits CTGF and Smad2/3 expression and proliferation of hepatic stellate cells. *Biotechnol Biotechnol Equip* **29**:124-131.

Li J, Pan Y, Kan M, Xiao X, Wang Y, Guan F, Zhang X and Chen L (2014) Hepatoprotective effects of berberine on liver fibrosis via activation of AMP-activated protein kinase. *Life Sci* **98**:24-30.

Liang Z, Li T, Jiang S, Xu J, Di W, Yang Z, Hu W and Yang Y (2017) AMPK: a novel target for treating hepatic fibrosis. *Oncotarget* **8**:62780-62792.

Lim JY, Oh MA, Kim WH, Sohn HY and Park SI (2012) AMP-activated protein kinase inhibits TGF-beta-induced fibrogenic responses of hepatic stellate cells by targeting transcriptional coactivator p300. *J Cell Physiol* **227**:1081-1089.

Puche JE, Saiman Y and Friedman SL (2013) Hepatic stellate cells and liver fibrosis. *Compr Physiol* **3**:1473-1492.

Schuppan D and Kim YO (2013) Evolving therapies for liver fibrosis. *J Clin Invest* **123**:1887-1901.

Thiele ND, Wirth JW, Steins D, Koop AC, Ittrich H, Lohse AW and Kluwe J (2017) TIMP-1 is upregulated, but not essential in hepatic fibrogenesis and carcinogenesis in mice. *Sci Rep* **7**:714.

Tripathi DM, Erice E, Lafoz E, Garcia-Caldero H, Sarin SK, Bosch J, Gracia-Sancho J and Garcia-Pagan JC (2015) Metformin reduces hepatic resistance and portal pressure in cirrhotic rats. *Am J Physiol Gastrointest Liver Physiol* **309**:G301-309.

Wang J, Wu X, Simonavicius N, Tian H and Ling L (2006) Medium-chain fatty acids as ligands for orphan G protein-coupled receptor GPR84. *J Biol Chem* **281**:34457-34464.

Wang N, Xu Q, Tan HY, Hong M, Li S, Yuen MF and Feng Y (2016) Berberine Inhibition of Fibrogenesis in a Rat Model of Liver Fibrosis and in Hepatic Stellate Cells. *Evid Based Complement Alternat Med* **2016**:8762345.

Weiler-Normann C, Herkel J and Lohse AW (2007) Mouse models of liver fibrosis. *Z Gastroenterol* **45**:43-50.

Wu YL, Zhang YJ, Yao YL, Li ZM, Han X, Lian LH, Zhao YQ and Nan JX (2016) Cucurbitacin E ameliorates hepatic fibrosis in vivo and in vitro through activation of AMPK and blocking mTOR-dependent signaling pathway. *Toxicol Lett* **258**:147-158.

Wynn TA (2007) Common and unique mechanisms regulate fibrosis in various fibroproliferative diseases. *J Clin Invest* **117**:524-529.

Xu J, Fu Y and Chen A (2003) Activation of peroxisome proliferator-activated receptor-gamma contributes to the inhibitory effects of curcumin on rat hepatic stellate cell growth. *Am J Physiol Gastrointest Liver Physiol* **285**:G20-30.

Yang H, Rudge DG, Koos JD, Vaidialingam B, Yang HJ and Pavletich NP (2013) mTOR kinase structure, mechanism and regulation. *Nature* **497**:217-223.

Yang Y, Zhao Z, Liu Y, Kang X, Zhang H and Meng M (2015) Suppression of oxidative stress and improvement of liver functions in mice by ursolic acid via LKB1-AMP-activated protein kinase signaling. *J Gastroenterol Hepatol* **30**:609-618.

Zhai X, Qiao H, Guan W, Li Z, Cheng Y, Jia X and Zhou Y (2015) Curcumin regulates peroxisome proliferator-activated receptor-gamma coactivator-1alpha expression by AMPK pathway in hepatic stellate cells in vitro. *Eur J Pharmacol* **746**:56-62.

Zhong J, Gong W, Chen J, Qing Y, Wu S, Li H, Huang C, Chen Y, Wang Y, Xu Z, Liu W, Li H and Long H (2018) Micheliolide alleviates hepatic steatosis in db/db mice by inhibiting inflammation and promoting autophagy via PPAR-gamma-mediated NF-small ka, CyrillicB and AMPK/mTOR signaling. *Int Immunopharmacol* **59**:197-208.

JPET Fast Forward. Published on August 9, 2018 as DOI: 10.1124/jpet.118.250068
This article has not been copyedited and formatted. The final version may differ from this version.
JPET#250068

Footnotes.

The authors declare competing financial interests: Research was funded by Prometic BioSciences inc. Authors are employees of Prometic BioSciences inc. and hold shares in Prometic Life Sciences inc.

JPET Fast Forward. Published on August 9, 2018 as DOI: 10.1124/jpet.118.250068
This article has not been copyedited and formatted. The final version may differ from this version.
JPET#250068

Figure Legends.

Figure 1. PBI-4050 reduces CCl_4-induced liver fibrosis. (a) Representative histological images of liver sections stained with Masson's trichrome of sham, CCl_4, or CCl_4 and PBI-4050 (200 mg/kg)-treated mice. (b) Quantification of Masson's trichrome stain of liver collagen deposition. (c) Hydroxyproline levels in liver tissue (d) Hepatic collagen I mRNA expression assessed by qPCR and (e) AST serum level. The column bar graphs represent the mean ± S.E.M. (sham, n=4; CCl_4 and CCl_4 + PBI-4050 at 100 or 200 mg/kg, n=10 each); * $p < 0.05$; ** $p < 0.01$; *** $p < 0.001$, by one-way ANOVA. Scale bars: 100 µm.

Figure 2. PBI-4050 reduces hepatic α-SMA in CCl_4-induced liver fibrosis model. (a) Representative immunohistochemical staining of α-SMA in liver sections. (b) Representative Western blot and densitometry analysis of α-SMA levels in liver lysates. (c) Hepatic α-SMA mRNA expression in liver tissue extracts. The column bar graphs represent the mean ± S.E.M. (sham, n=4; CCl_4 and CCl_4 + PBI-4050 at 200 mg/kg, n=10 each); * $p < 0.05$; ** $p < 0.01$, by one-way ANOVA. Scale bars: 200 µm.

Figure 3. Effect of PBI-4050 on expression of fibrosis and oxidative stress markers and receptors in liver tissue. Hepatic mRNA expression of (a) MMP2, (b) TIMP-1, (c) Snail1, (d) iNOS (*Nos2*), (e) PPARγ, and (f) GPR84 assessed by qPCR. Data represent the mean ± S.E.M. (sham, n=4; CCl_4 and CCl_4 + PBI-4050 at 100 or 200 mg/kg, n=10 each); * $p < 0.05$; ** $p < 0.01$; *** $p < 0.001$, by one-way ANOVA.

JPET Fast Forward. Published on August 9, 2018 as DOI: 10.1124/jpet.118.250068
This article has not been copyedited and formatted. The final version may differ from this version.

Figure 4. PBI-4050 reduces bile duct ligation-induced hepatic fibrosis in rats. (a) Representative histological images of liver sections stained with Sirius red; (b) digital image analysis of liver fibrosis area; (c, d) Western blot (c) and densitometry analysis (d) of α-SMA levels in liver lysates. (sham, n=5; BDL, n= 7; BDL + PBI-4050, n = 6) * $p < 0.05$; ** $p < 0.01$, by one-way ANOVA. Scale bars: 200 µm.

Figure 5. Anti-proliferative effect of PBI-4050 on activated HSCs. (a) Cell proliferation of HSCs treated for 24h with 10 ng/mL of TGF-β1 and PBI-4050 at 250 or 500 µM was assessed by Resazurin reduction at 0 and 24h. Results are the mean ± S.E.M. of 3 independent experiments; * $p < 0.05$; *** $p < 0.001$, by one-way ANOVA. (b) HSCs were treated as described above and cell cycle analyzed by flow cytometry. Percentage of cells in G0/G1, S, G2/M and apoptosis phases of the cell cycle are shown.

Figure 6. PBI-4050 abbrogates fibrogenic markers in activated HSCs. (a) mRNA expression of activated-stellate cell markers α-SMA, pro-fibrotic marker CTGF and PPARɣ were determined in TGF-β1-stimulated HSCs treated with PBI-4050 at 250 µM or 500 µM for 24 hours. (b, c) Representative Western blot and densitometry analysis of α-SMA protein level was assessed by Western Blot (b) and secreted protein levels of pro-fibrotic CTGF was measured in cell supernatant by ELISA (c). Data represent the mean ± S.E.M. of 3 independent experiments; ** $p < 0.01$; *** $p < 0.001$, by one-way ANOVA.

Figure 7. PBI-4050 increases AMPK and LKB1 phosphorylation, and inhibits mTOR activation and intracellular ATP levels in HSCs. HSCs were treated for 24h with TGF-β1 (10 ng/mL) in the presence or absence of PBI-4050. Western blot was performed to quantify total and phosphorylated AMPK (a), LKB1 (b), and mTOR (c) protein levels. Ratios of p-AMPKα/AMPK, p-LKB1/LKB1, and p-mTOR/mTOR were determined. (d) Intracellular ATP levels. The column bar graphs represent the mean ± S.E.M. of 3 independent experiments; * $p < 0.05$; ** $p < 0.01$; *** $p < 0.001$, by one-way ANOVA.

JPET Fast Forward. Published on August 9, 2018 as DOI: 10.1124/jpet.118.250068
This article has not been copyedited and formatted. The final version may differ from this version.

Figure 8. A schematic representation showing the protective effect of PBI-4050 on hepatic fibrosis. PBI-4050 decreases intracellular ATP level and activates LKB1, one of the upstream kinases phosphorylating AMPK. In turn, activated AMPK and low ATP levels can inhibit the cell growth master regulator mTOR and thereby restore PPARγ expression, leading to inhibition of HSC activation and proliferation. Consequently, fibrotic and remodeling markers are decreased by PBI-4050, resulting in improvement of hepatic fibrosis.

Figure 1

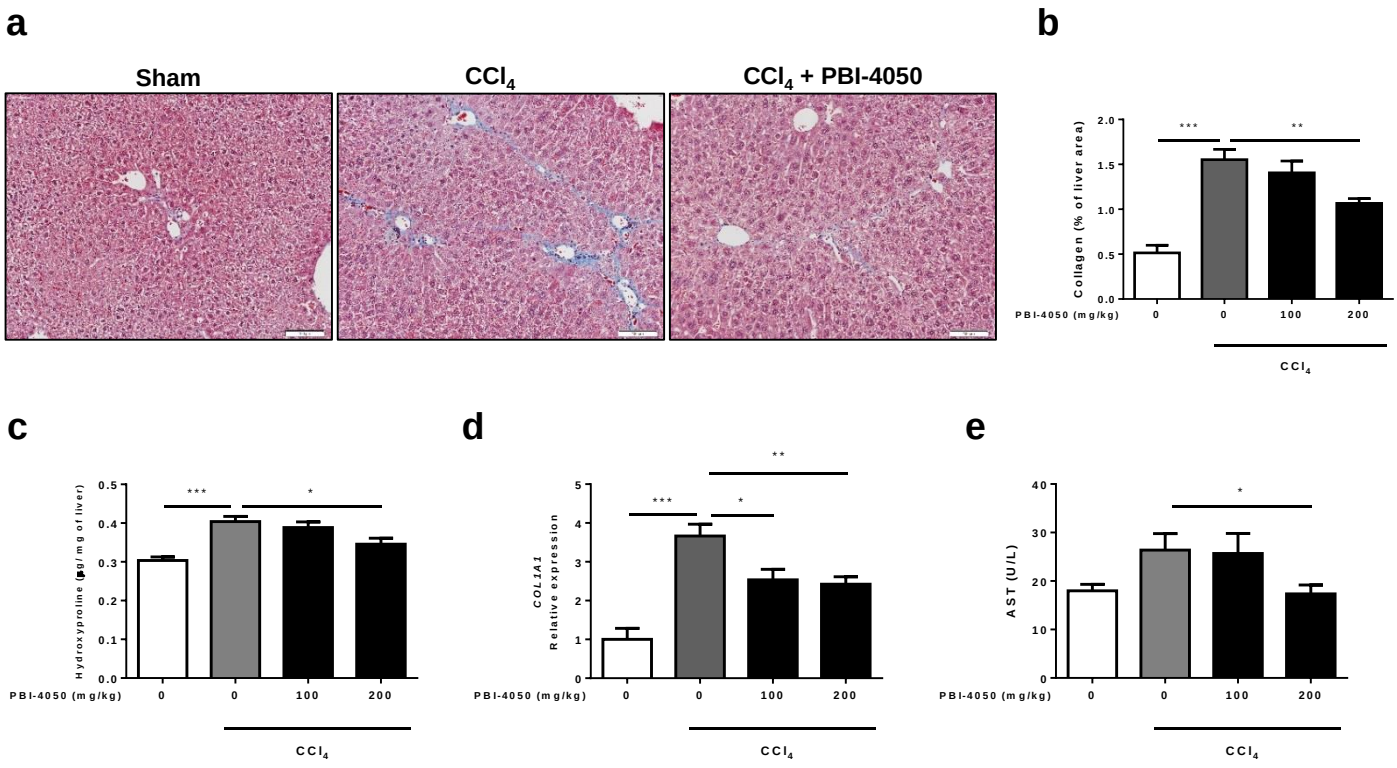
a
Sham
CCl4
CCl4 + PBI-4050
b
Collagen (% of liver area)
***
**
PBI-4050 (mg/kg)
0
0
100
200
CCl4
c
Hydroxyproline (μg/mg of liver)
***
*
PBI-4050 (mg/kg)
0
0
100
200
CCl4
d
COL1A1
Relative expression
**
***
*
PBI-4050 (mg/kg)
0
0
100
200
CCl4
e
AST (U/L)
*
PBI-4050 (mg/kg)
0
0
100
200
CCl4

Figure 2

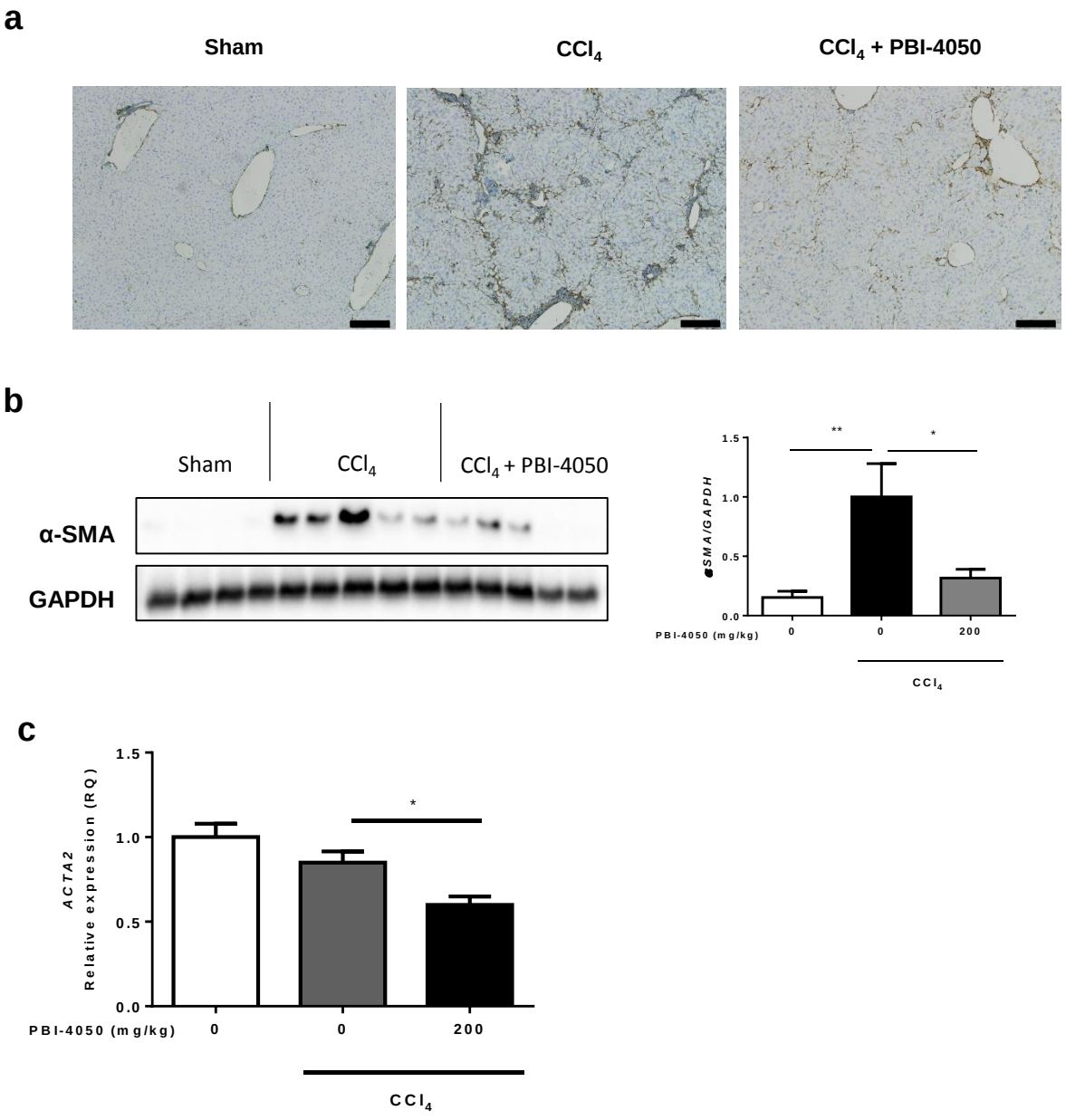
a
Sham
CCl4
CCl4 + PBI-4050
b
Sham
CCl4
CCl4 + PBI-4050
α-SMA
GAPDH
αSMA/GAPDH
1.5
1.0
0.5
0.0
**
*
PBI-4050 (mg/kg)
0
0
200
CCl4
c
ACTA2
Relative expression (RQ)
1.5
1.0
0.5
0.0
*
PBI-4050 (mg/kg)
0
0
200
CCl4

Figure 3

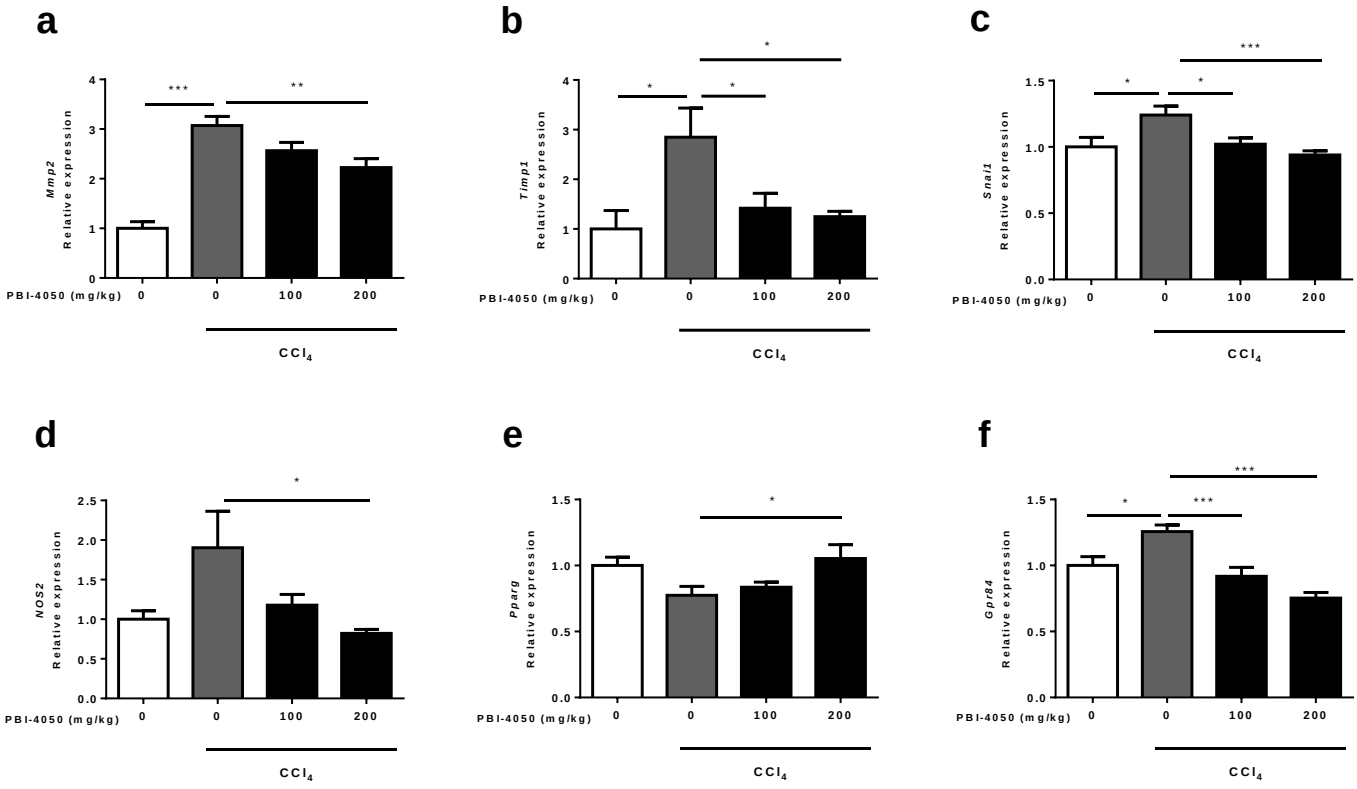
a
b
c
d
e
f
Mmp2
Timp1
Snai1
NOS2
Pparg
Gpr84
Relative expression
PBI-4050 (mg/kg)
0
0
100
200
CCl4
***
**
*

Figure 4

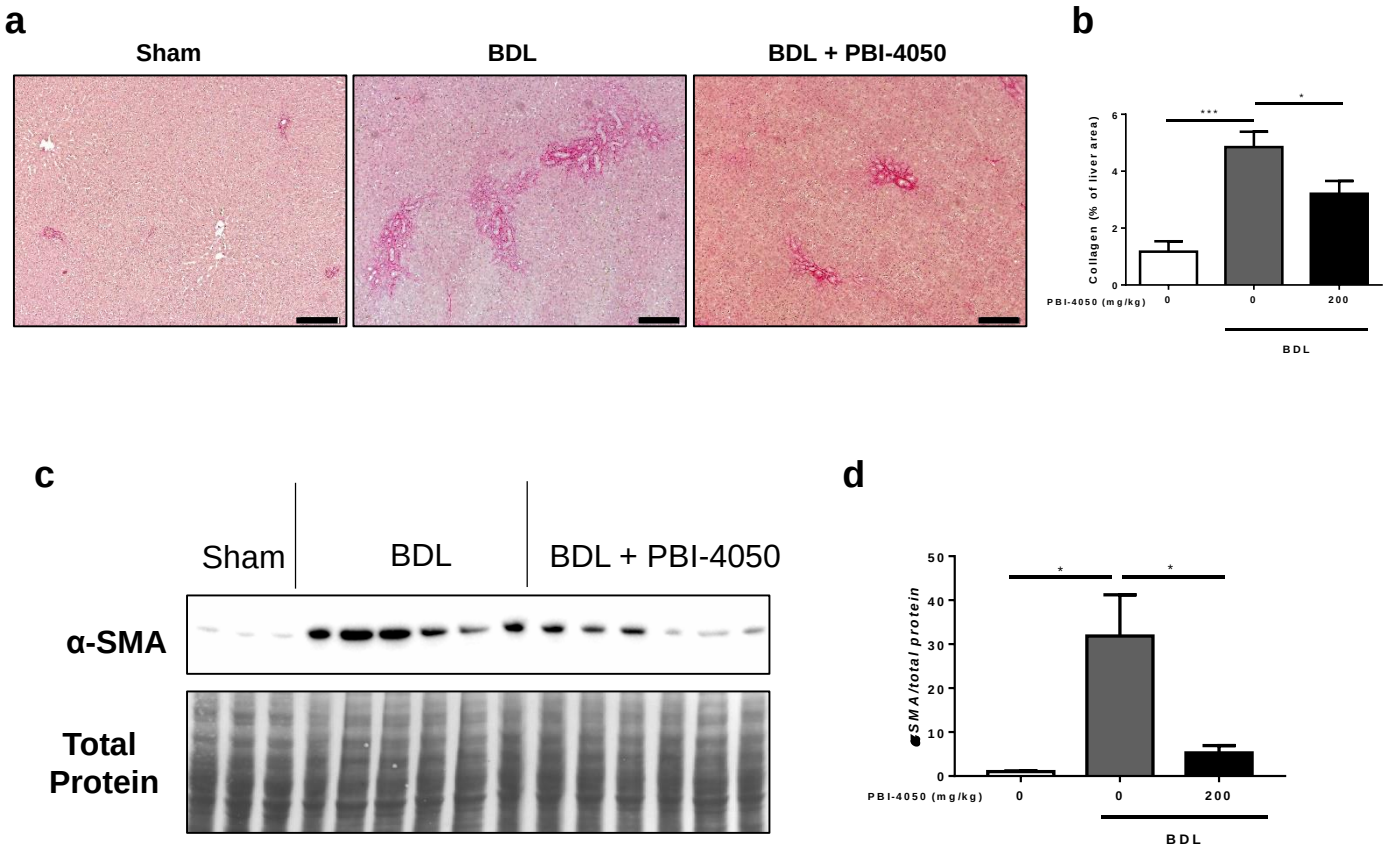
a
Sham
BDL
BDL + PBI-4050
b
Collagen (% of liver area)
***
*
PBI-4050 (mg/kg)
0
0
200
BDL
c
Sham
BDL
BDL + PBI-4050
α-SMA
Total Protein
d
αSMA/total protein
*
*
PBI-4050 (mg/kg)
0
0
200
BDL

Figure 5

a

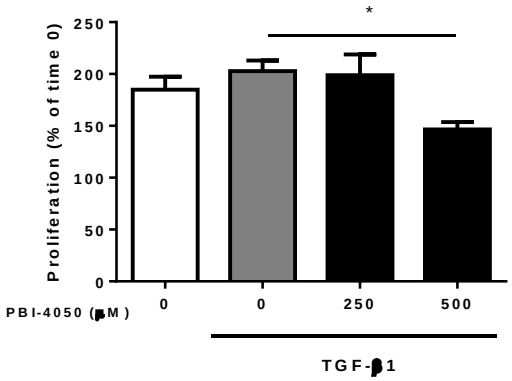
*
Proliferation (% of time 0)
250
200
150
100
50
0
PBI-4050 (µM)
0
0
250
500
TGF-β1

b

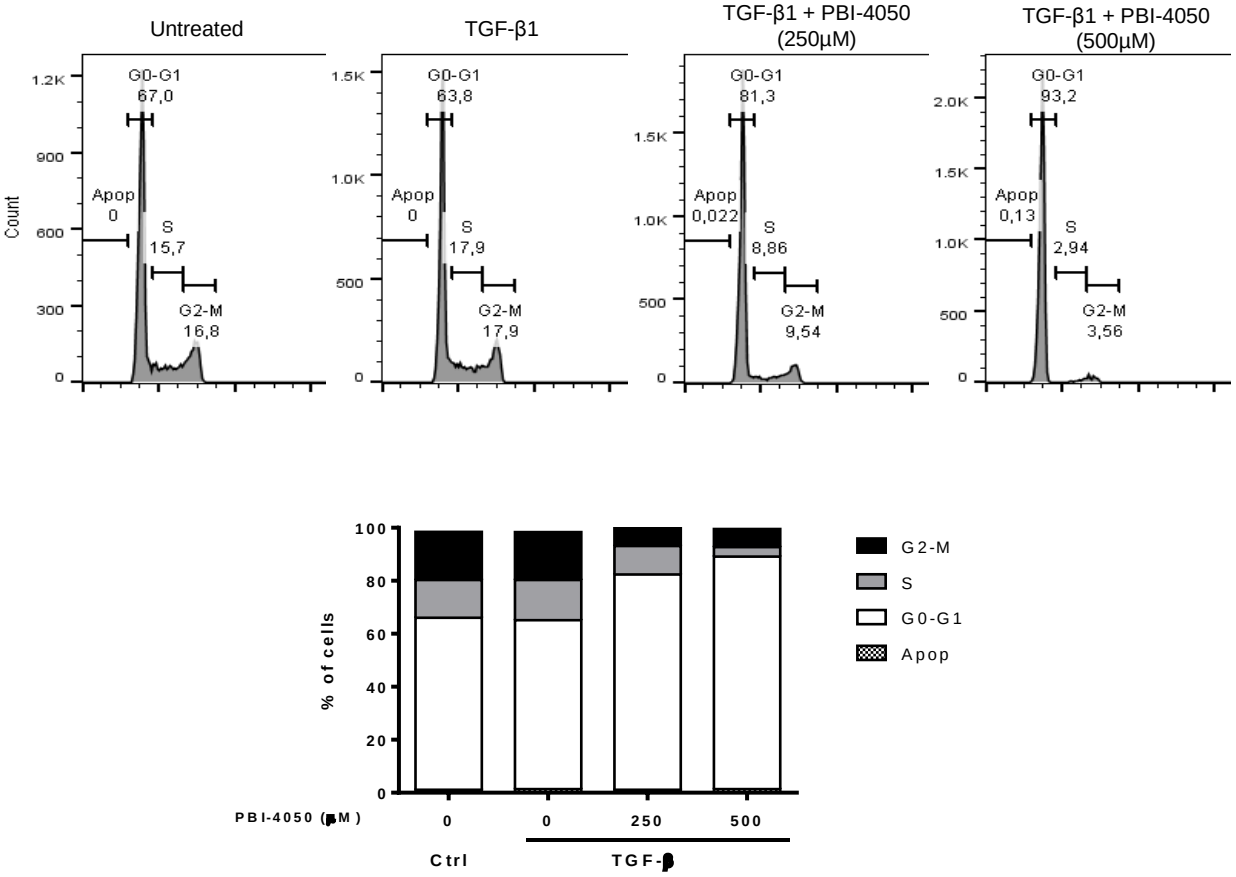
Untreated
TGF-β1
TGF-β1 + PBI-4050 (250µM)
TGF-β1 + PBI-4050 (500µM)
Count
G0-G1 67,0
Apop 0
S 15,7
G2-M 16,8
G0-G1 63,8
Apop 0
S 17,9
G2-M 17,9
G0-G1 81,3
Apop 0,022
S 8,86
G2-M 9,54
G0-G1 93,2
Apop 0,13
S 2,94
G2-M 3,56
% of cells
G2-M
S
G0-G1
Apop
PBI-4050 (µM)
0
0
250
500
Ctrl
TGF-β

Figure 6

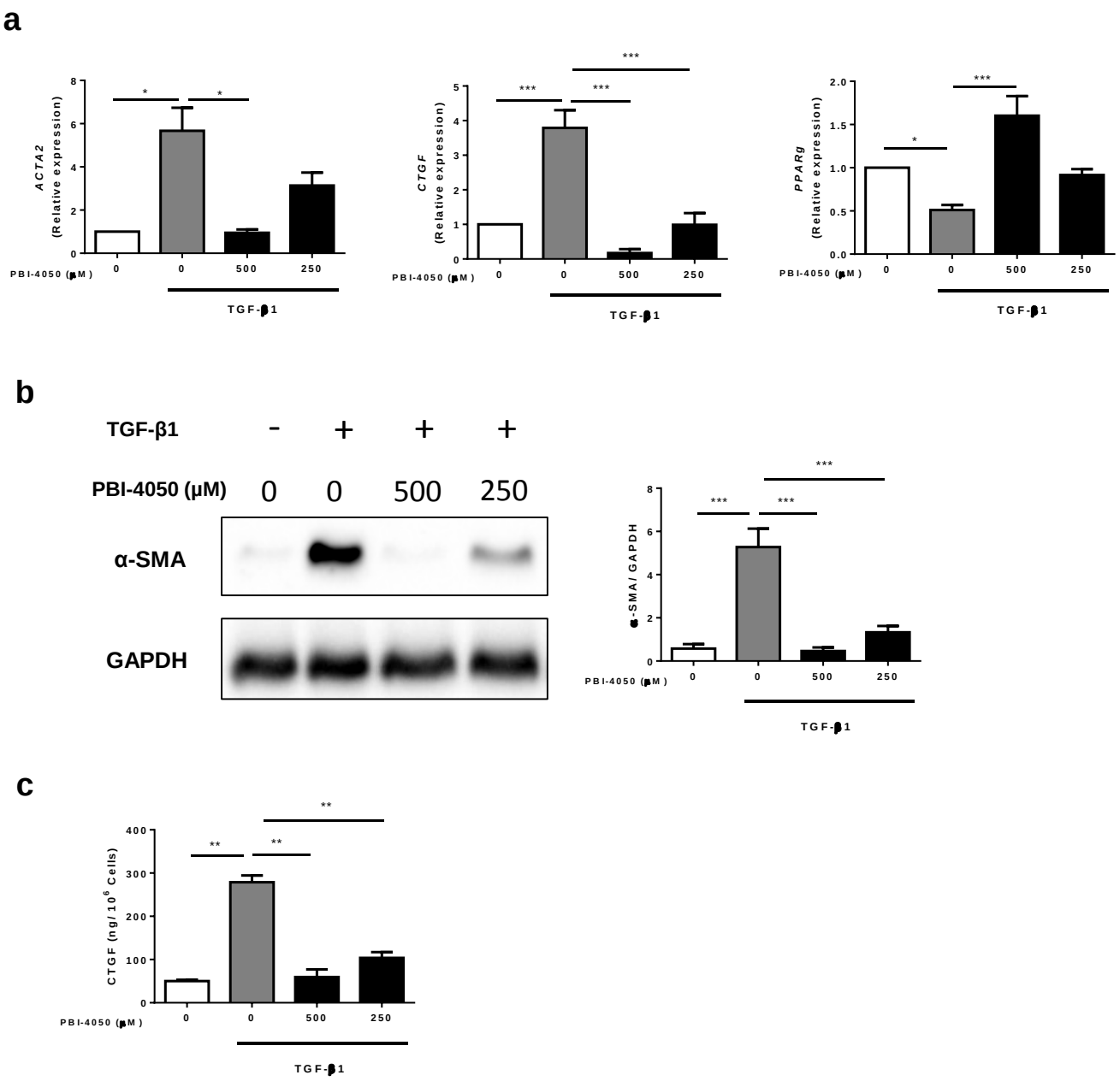
a
ACTA2 (Relative expression)
CTGF (Relative expression)
PPARg (Relative expression)
PBI-4050 (μM)
0
0
500
250
TGF-β1
b
TGF-β1 - + + +
PBI-4050 (μM) 0 0 500 250
α-SMA
GAPDH
α-SMA/ GAPDH
c
CTGF (ng/10^6 Cells)

Figure 7

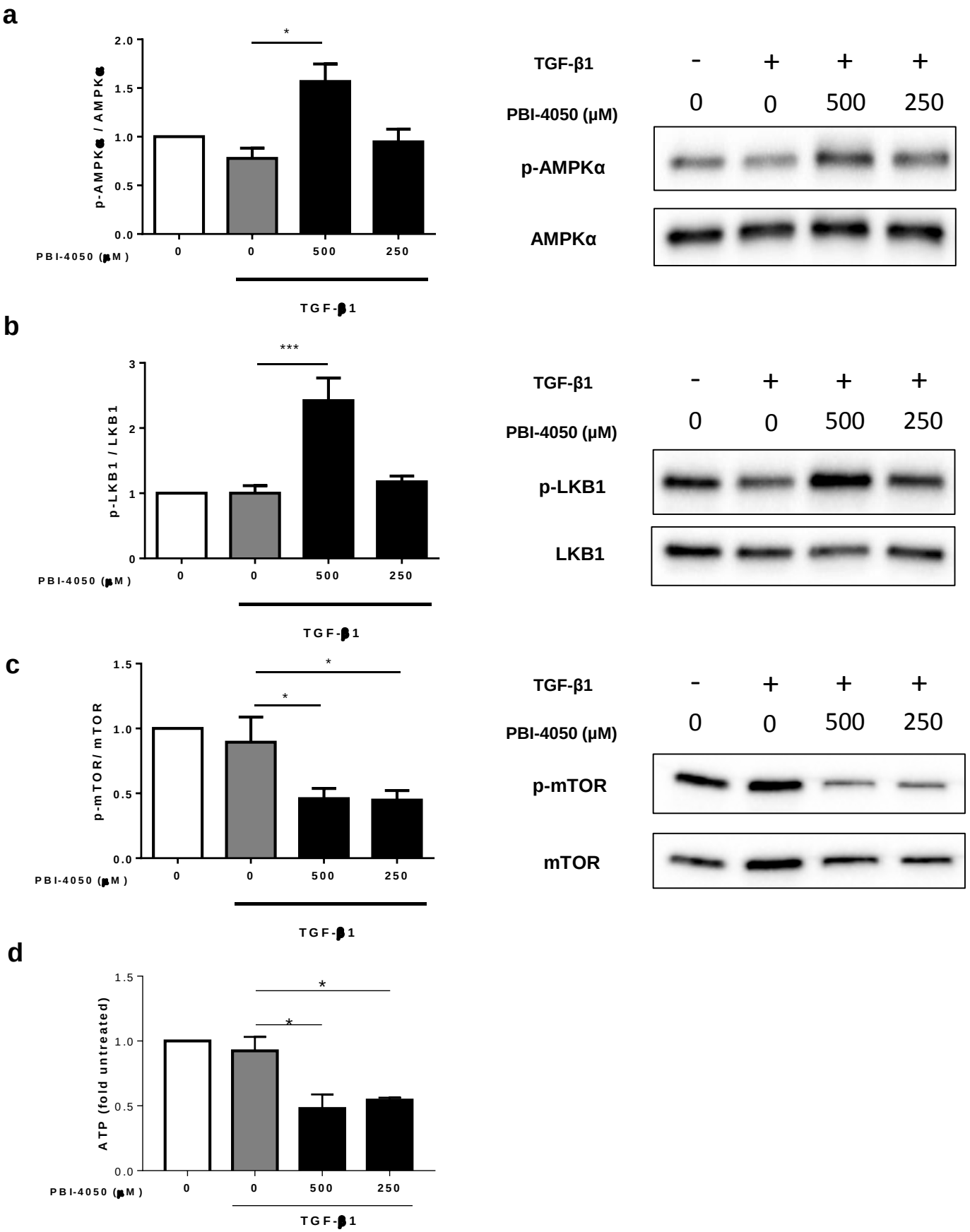
a
p-AMPKα / AMPKα
2.0
1.5
1.0
0.5
0.0
*
PBI-4050 (μM)
0
0
500
250
TGF-β1
TGF-β1
-
+
+
+
PBI-4050 (μM)
0
0
500
250
p-AMPKα
AMPKα
b
p-LKB1 / LKB1
3
2
1
0
***
PBI-4050 (μM)
0
0
500
250
TGF-β1
TGF-β1
-
+
+
+
PBI-4050 (μM)
0
0
500
250
p-LKB1
LKB1
c
p-mTOR/ mTOR
1.5
1.0
0.5
0.0
*
*
PBI-4050 (μM)
0
0
500
250
TGF-β1
TGF-β1
-
+
+
+
PBI-4050 (μM)
0
0
500
250
p-mTOR
mTOR
d
ATP (fold untreated)
1.5
1.0
0.5
0.0
*
*
PBI-4050 (μM)
0
0
500
250
TGF-β1

Figure 8

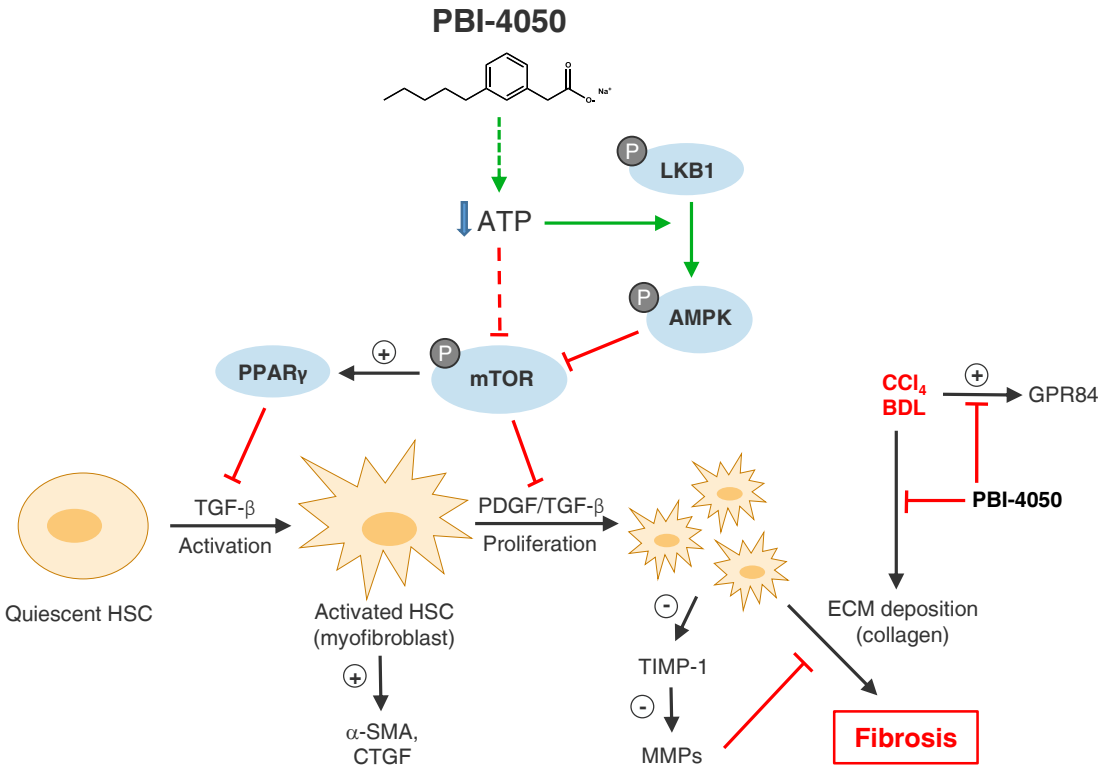
PBI-4050
LKB1
ATP
AMPK
mTOR
PPARγ
CCl4
BDL
GPR84
PBI-4050
TGF-β
Activation
PDGF/TGF-β
Proliferation
Quiescent HSC
Activated HSC
(myofibroblast)
α-SMA,
CTGF
TIMP-1
MMPs
ECM deposition
(collagen)
Fibrosis

Supplemental data

PBI-4050 reduces stellate cell activation and liver fibrosis through modulation of intracellular ATP levels and LKB1-AMPK-mTOR pathway

Brigitte Grouix, Francois Sarra-Bournet, Martin Leduc, Jean-Christophe Simard, Kathy Hince, Lilianne Geerts, Alexandra Blais, Liette Gervais, Alexandre Laverdure, Alexandra Felton, Jonathan Richard, Jugurtha Ouboudinar, William Gagnon, François Leblond, Pierre Laurin and Lyne Gagnon

The Journal of Pharmacology and Experimental Therapeutics

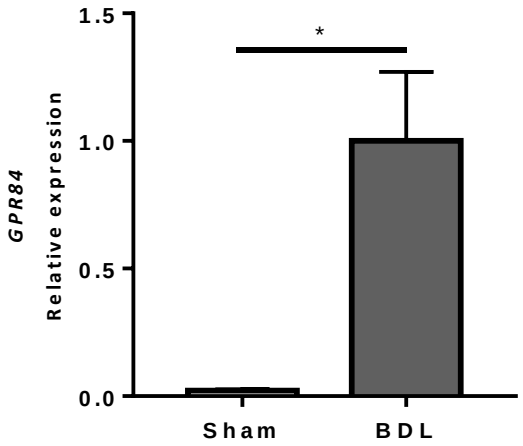

Supplemental Figure 1. Induction of GPR84 expression in the bile-duct ligation rat model. GPR84 mRNA expression was quantified by qPCR. Data represent the mean ± S.E.M. of 3 experiments; * $p < 0.05$ (two-tailed Student's T test).

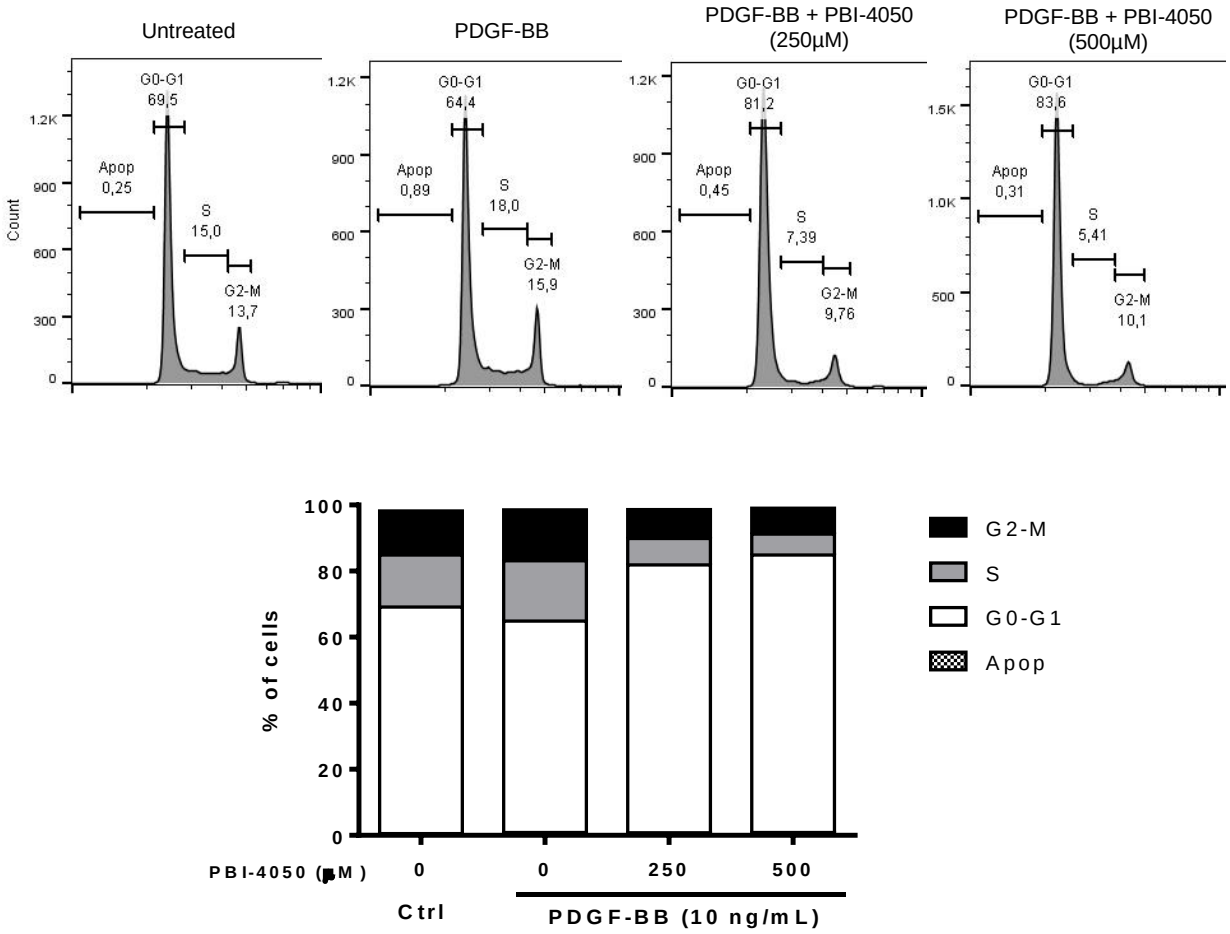

Supplemental Figure 2. Anti-proliferative effect of PBI-4050 on activated HSCs. Cell cycle was analyzed by flow cytometry on HSCs treated for 24h with 10 ng/mL of PDGF-BB with or without PBI-4050 at 250 or 500 µM. Histograms are from one representative out of 3 independent experiments. Contingency graph are means of 3 experiments. Percentage of cells in G0/G1, S, G2/M and apoptosis phases of the cell cycle are shown.

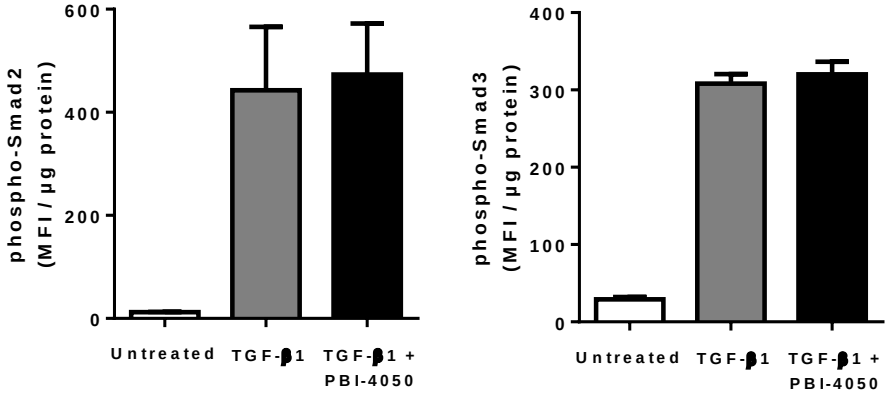

Supplemental Figure 3. PBI-4050 does not modulate TGF-β1-induced Smad2 and Smad3 phosphorylation. Human Hepatic Stellate cells were starved in medium without FBS for 4h and treated for 20 minutes with TGF-β1 (10 ng/ml) in the presence or absence of PBI-4050 (500 µM). Cell lysates were analyzed for changes in phosphorylated Smad2 (Ser465/Ser467) and Smad3 (Ser423/Ser425) using the MILLIPLEX MAP Human TGFβ Signaling Magnetic Bead Panel. Mean Fluorescence Intensity (MFI) results were normalized to protein concentration in cell lysates. Results represent the mean ± S.E.M. of 2 independent experiments.

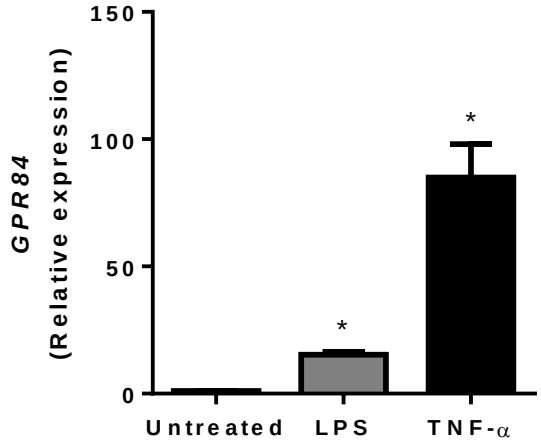

Supplemental Figure 4. Induction of GPR84 mRNA expression by LPS and TNFα. Human Hepatic Stellate cells were starved in 0.4% FBS medium for 4h and treated for 5 hours with LPS (100 ng/mL) and TNFα (50 ng/mL). GPR84 mRNA expression was quantified by qPCR. Data represent the mean ± S.E.M. of 3 experiments; * $p < 0.05$ treatment vs untreated by one-way ANOVA.